Methods Brief/

A Low-Cost Programmable Reversing Flow Column Apparatus for Investigating Mixing Zones

Reid. E. Buskirk

Corresponding author: Department of Geology and Geophysics, Texas A&M University, College Station, TX, 77843, USA, reid_buskirk@tamu.edu

Peter. S. K. Knappett

Department of Geology and Geophysics, Texas A&M University, College Station, TX, 77843, USA, knappett@tamu.edu

Meinhard Bayani. Cardenas

Jackson School of Geosciences, The University of Texas at Austin, Austin, TX, 78712-1692, cardenas@jsg.utexas.edu

Saugata. Datta

Department of Earth and Planetary Sciences, University of Texas at San Antonio, TX 78249, saugata.datta@utsa.edu

Walter. S. Borowski

Department of Physics, Geosciences, and Astronomy, Eastern Kentucky University, Richmond, KY, 40475 USA, w.borowski@eku.edu

Itza Mendoza-Sanchez

Department of Environmental and Occupational Health, Texas A&M University, College Station, TX, 77843, USA, itzamendoza@tamu.edu

Declaration of Competing Interest

The authors declare that they have no known competing financial interests or personal relationships that could have appeared to influence the work reported in this paper.

Keywords: Column Experiment, Mixing Zones, Groundwater Surface Water Interfaces, Physical Model

Article Impact Statement:

We developed a low-cost programable column experiment apparatus capable of automating reversing flows a range of flux magnitudes.

Abstract

This note describes the development and testing of a novel, programmable reversing flow 1D (R1D) experimental column apparatus designed to investigate reaction, sorption, and transport of solutes in aquifers within dynamic reversing flow zones where waters with different chemistries mix. The motivation for constructing this apparatus was to understand the roles of mixing and reaction on arsenic discharging through a tidally fluctuating riverbank. The apparatus can simulate complex transient flux schedules similar to natural flow regimes The apparatus uses an Arduino microcontroller to control flux magnitude through two peristaltic pumps. Solenoid valves control flow direction from two separate reservoirs. In-line probes continually measure effluent electrical conductance, pH, oxidation-reduction potential, and temperature. To understand how sensitive physical solute transport is to deviations from the real hydrograph of the tidally fluctuating river, two experiments were performed using: 1) a simpler constant magnitude, reversing flux direction schedule (RCF); and 2) a more environmentally relevant variable magnitude, reversing flux direction schedule (RVF). Wherein, flux magnitude was ramped up and down according to a sine wave. Modeled breakthrough curves of chloride yielded nearly identical dispersivities under both flow regimes. For the RVF experiment, Peclet numbers captured the transition between diffusion and dispersion dominated transport in the intertidal interval. Therefore, the apparatus accurately simulated conservative, environmentally relevant mixing under transient, variable flux flow regimes. Accurately generating variable flux reversing flow regimes is important to simulate the interaction between flow velocity and chemical reactions where Brownian diffusion of solutes to solid-phase reactions sites is kinetically limited.

Introduction

Dynamic reversing flow conditions can drive mixing zones between waters with disparate chemistries in both natural and human-impacted aquifers. Within these mixing zones, hydrological and biogeochemical processes are coupled in ways that mediate metal and nutrient reactions. This coupling can significantly alter the chemistry of water that passes through these zones. Examples of dynamic reversing zones include: 1) oscillating water tables within aquifers **(Du Laing et al. 2009; Rezanezhad et al. 2014; Wang et al. 2017**); 2) push-pull tests performed on monitoring wells below the water table **(Kruisdijk and van Breukelen, 2021; Radloff et al.. 2017, 2011; Teutsch et al. 2005**); 3) riverbanks and riverbeds of dynamically fluctuating rivers **(Benner et al. 2008; Berube et al. 2018; Datta et al. 2009; Jung et al. 2015; Rhodes et al. 2017; Xu et al. 2017; Zachara et al.** 2013); 4) estuarine beds **(Geng et al. 2021; Michael et al. 2003; Spiteri et al. 2008)**; and 5) salt water beaches **(Kim et al. 2017; McAllister et al. 2015). The latter** are commonly impacted by storm surges and ocean tides. Isolating the individual and collective impacts of physical transport with kinetically limited and equilibrium limited biochemical reactions within mixing zones is important for predicting water quality, as well as ecosystem and human health. Prior studies of these mixing zones routinely note the need to elucidate the impacts of transient flow and biochemical reactions on metal and nutrient transport in these interfaces **(Berube et al. 2018; Bone et al. 2006; Datta et al. 2009; Hester et al. 2017; Parsons et al. 2013; Sawyer et al. 2009; Xu et al. 2017; Zachara et al. 2013)**. However, few experimental apparatuses have been developed to achieve this. Dynamic reversing flow mixing zones are notoriously difficult to study. Field studies on transport and reaction in mixing zones face challenges of representative sampling without inducing artificial mixing (Hester et al. 2017) and identifying the flow pathway in 3-Dimensions (3-D) too perform mass balance calculations of reactants and products of biochemical reactions. Numerical models offer the power of process-level insights into transport and reaction within mixing zones. However, these models often

require assumptions for many unconstrained parameters, which leads to generating non-unique solutions.

Physical scale models of mixing zones in laboratory settings inherently require simplified conditions relative to the field. However, physical models permit control over the flux regimes, sediment compositions, and influent chemistries. This control enables fine-scale temporal and spatial sampling and observations to constrain key chemical reactions and physical transport processes that are otherwise difficult to discern from field and modeling studies. Hence, physical models can help constrain the hydrological (porewater residence time, mixing of disparate end-members, timing and magnitude of flow reversals) and biogeochemical (redox chemistry, solid-phase chemistry, biochemical reaction kinetics and equilibrium reactions) mechanisms of contaminant transport to and from dynamic reversing mixing zones (Li et al.. 2020; Liu et al.. 2017; Rezanezhad et al.. 2014; Ziliotto et al.. 2021). If implemented in conjunction with a field study, these physical models can potentially isolate site-specific chemical reactions, thereby helping to explain spatial and temporal patterns in pore-water chemistry in the field and helping to constrain numerical models.

Despite their potential, there are few published examples of laboratory scale physical models of dynamic reversing mixing zones. This lack of physical models may be owed to the lack of a cost-effective and adaptable general-purpose apparatus. Physical model applications that have been described in publications include devices that simulate push pull tests and multi-well remediation (Sather et al. 2023), apparatuses simulating oscillating water tables (Rezanezhad et al. 2014; Xin et al. 2018) and reversing flow 1D column experiments (Li et al. 2020; Liu, et al. 2017).

Reversing flow, 1D column experiments (R1D) present a potentially flexible, cost-effective and reproducible approach (Li et al.. 2020; Liu, et al.. 2017). Past R1D- experiments implemented constant fluxes with abrupt flow reversals between influent and effluent ends of the column (Li et al.. 2020; Liu, et al.. 2017). Transient flow behavior, however, is inherent to dynamic reversing mixing zones. During faster flow conditions, advective transport dominates, whereas during more stagnant conditions, diffusive transport dominates. The kinetics of adsorption and desorption (Nkedi-Kizza et al. 1984), and mineral growth and dissolution (Berner, 1978; Drever, 1997) mechanisms all have Brownian diffusion steps that could be favored by slower flow conditions. Moreover, local thermodynamic chemical equilibrium may be approached under slow flow conditions which may slow reactions compared to faster flow rates where the reactants are quickly delivered, and the products are quickly removed from the reaction sites. Under higher flow rate conditions then, nonequilibrium kinetics may govern the completeness of reactions along the flow path (Bearup et al.. 2012). Hence, R1D apparatuses could help investigate how coupled transient flow and geochemical reactions control contaminant transport behavior at real world sites.

For example, we could determine the mechanisms behind how Fe-oxide Permeable Natural Reactive Barriers (PNRB) accumulate solid-phase As from discharging groundwater along the tidally fluctuating Meghna River, Bangladesh. This process has been proposed to produce the high solid-phase concentrations of As (>23,000 mg/kg) associated with Fe-oxides in 1-2 m deep riverbank sediments (Datta et al., 2009). The process has been investigated at numerous field sites by measuring hydraulic gradients, pore-water chemistry and volumetric fluxes (Jung et al., 2015; Berube et al., 2018; Huang et al. 2022). The PNRBs are likely maintained by the fluctuating position of a redox gradient that spans a mixing zone between

anerobic groundwater to aerobic surface water. Direct observations are lacking of As attaching to Fe-oxide surfaces that form under oscillating river stage conditions. Little is known on whether Fe-oxides recrystallize into more stable crystalline mineralogies, permitting the PNRB to persist during the wet season when the riverbank is fully inundated. Dam building and sea level rise may further impact the stability of Fe-oxide deposits and their metal sorbents.

The development of an R1D can simulate the real-world flow regimes, using sediment cores from riverbanks to answer these questions. To the authors' knowledge, a transient R1D apparatus and experiment has not been attempted to mimic the gradual transition between high and low flow rates inherent in real-world dynamic mixing zones. This is important to capture the transition between equilibrium and nonequilibrium kinetics.

We present a first-of-its kind experimental apparatus, in the form of a programable R1D column apparatus that can simulate transient dynamic reversing mixing zones. The automation of most processes within this apparatus minimizes past logistical hurdles such as having to manually adjust manual flow rates and turn valves. This automation permits the operator(s) more time for sample processing and analyses. Cost-effective tools, parts, and software were intentionally selected to encourage the reproduction of this apparatus in other institutions.

The objective of this study was to produce an environmentally relevant reversing flow regime that mimics the variable flux magnitude and direction that is seen in transiently fluctuating rivers. Two experiments were performed on the same packed sediment column using: a simpler constant magnitude, reversing flux direction flow regime (RCF); and the more environmentally relevant variable magnitude, reversing flux direction regime (RVF) in which flux magnitude was ramped up and down according to a sine wave discretized at 30 second time-steps. To confirm the apparatus simulated this more complex RVF flow regime with high

accuracy, the breakthrough curves of both experiments were fit to sediment dispersivity using a 1-D numerical model. Identical boundary conditions were imposed in the numerical model as input into the R1D sediment column. If the RVF flow regime was accurate, similar dispersivities are expected.

Materials and Methods

The R1D apparatus alternatively injects water from two separate reservoirs into opposing ends of a column filled with sediment analogously to real-world dynamic reversing zones (Fig. 1). In the example shown in Figure 1, artificial groundwater (AGW) is injected into the column through one end, displacing artificial surface water (ASW) that is already in the column (Fig. 1a). When flow direction is reversed, ASW then displaces AGW through the opposite end of the column (Fig. 1b). The column effluent passes through a set of in-line water quality probes before collection.

We simulated the two different flow regimes with the apparatus (Fig. 1c-d). In the first experiment, the flow rate was held constant over a 6 hr interval before a full reversal. The flow regime in this first experiment is comparable to flow regimes used in prior R1D experiments by Liu et al. (2017) and Li et al. (2020). In the second experiment, at the start of each interval, the flow rate was gradually ramped up and then down again as the next reversal approached the end of the interval. This ramping flow rate approximated the sine wave of a semi-diurnally fluctuating river stage centered on zero with a riverbank aquifer that has a relatively constant water table compared to the fast-changing river stage (Fig. 1c-d) (Berube et al. 2018; Shuai et al. 2017).The different flow regimes in the column were controlled by an programable Arduino microcontroller that modulated flux from a pair of peristaltic pumps at 30 second intervals. The

source of influent water and the corresponding direction of flow through the column was controlled by a set of 3-way diverting valves.

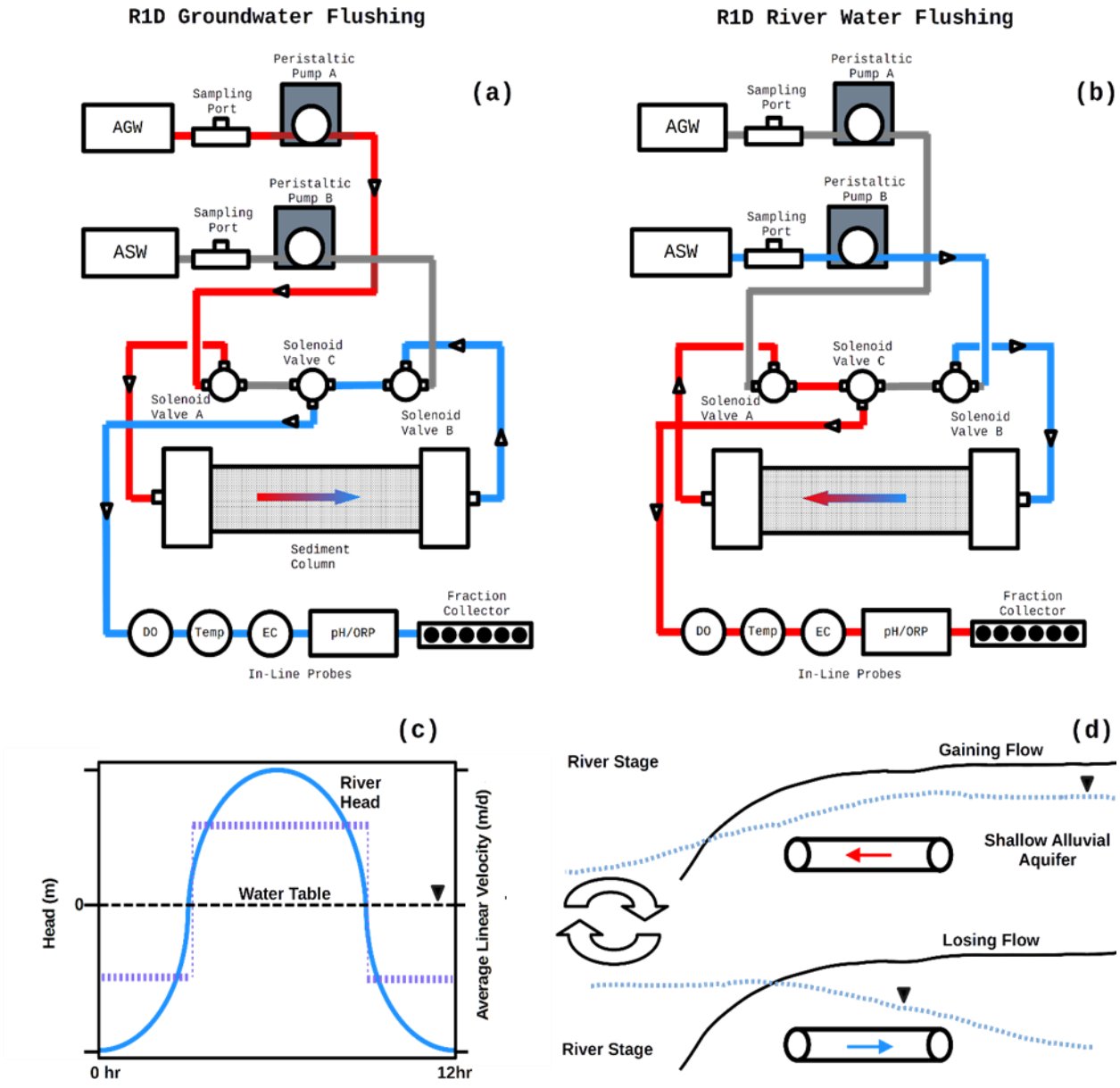

Figure 1. Tubing connections and flow pathways within the R1D apparatus are illustrated. Artificial groundwater and artificial surface water chemistries are represented by the colors red and blue, respectively. (a) Artificial groundwater injection stage. (b) Artificial surface water injection stage following a reversal in flow direction. (c) Two different flow regimes

approximating a tidal pulse signal. The constant and variable flux regime temporal pattern in flux (and driving head) are represented by purple and blue, respectively. (d) Conceptual model that shows the location of the sediment column in the riverbank and the hydraulic gradients during gaining and losing conditions.

Plumbing and Electronics

The Arduino Due was connected to a computer to receive programs to run the experiments and to log timestamp, pore volume (PV) estimates, and inline probe measurements. The volumetric flux of two low flow (0.005-32 mL/min) variable-speed peristaltic pumps (Model BQ80S, Golander Pump, Norcross GA USA) was controlled by the digital to analog 12-bit output pin of the Arduino. The output voltage range was expanded from 0.55-2.75 V to 0-3.3 V using a dual power LM358 operational amplifier (LM358, Texas Instruments, Dallas TX USA). The three 12V DC PTFE solenoid diverting valves (2552N14, McMaster Carr, Elmhurst, IL) were actuated with a relay module using an electronically isolated power source. The solenoid valves were negative voltage spike compensated with flyback diodes (Model 1N4007, Ltvystore Seattle WA USA). A complete wiring diagram and parts list of the apparatus is provided in the supplemental material **(**Table S1; Fig. S2**).** Total material expenditures for the apparatus were $3515.62 USD (2021) and the parts list is reported in SI 2.

The Arduino Due controlled flux by modulating voltage to the pump's serial port with the variable digital to analog (DAC) pin, modified to a working 0-3.3 V range. However, the relationship between input voltage and the volumetric water flux produced by the peristaltic pumps needed to be calibrated. Observed fluxes were manually calibrated against input voltages from the R1D prior to the experiments **(**Fig. S3**).** The accuracy of the flux was verified by

weighing the mass of water recovered and comparing that mass to that predicted by the calibrated variable flow rates.

In-Line Probes and Measurements

In-line temperature, electrical conductivity (EC), pH, and oxidation-reduction potential (ORP) probes were installed in custom-made acrylic flow cells downstream of the column effluent. These flow cells had vertically oriented inlet and outlet ends to prevent the buildup of air, which can interfere with the probes. The volume of the flow cells was kept low to minimize mixing prior to sampling the effluent. Including effluent tubing and flow cells, the total downstream dead volume was 4.36 mL. Unless otherwise noted, all the following probes and materials were purchased from Atlas Scientific (Long Island City, NY). The EC probe was an Atlas Scientific Mini 1.0 EC and was two-point calibrated with 88 µS/cm (Biopharm, Hatfield AR) and 1413 µS/cm solutions. A Micro pH Probe was calibrated at the start of the experiment using pH buffers of 4, 7, and 10. A Micro ORP Probe was calibrated using a 225 mV (Zobell's) solution. The computer logged the probe data from the Arduino into a comma delimited file using the software puTTY (Version 0.76) (Tatham, 2021). In-line temperature, pH, EC, and ORP were measured at a 30 second frequency.

Column Experiment Preparation

To improve the reproducibility between separate experiments and to prevent air bubbles from being trapped in pore spaces, the column was wet packed similarly to prior column experiment studies with homogenously packed sand (Brush et al. 1999; Lewis and Sjöstrom, 2010) (Appendix S1). Angular, well sorted, medium sized silica sand (> 98.7% silica) was used

(HM-108, Gilson Company Inc, Lewis OH USA). The median (d_{50}), tenth percentile, (d_{10}), and sixtieth percentile (d_{60}) grain size diameters were of 359 µm, 190 µm and 389 µm, respectively (Appendix S1). The cylindrical acrylic column had a length of 20 cm and an inner diameter of 6.30 cm (Knappett et al. 2008). When wet packed, sand was slowly added to a column partially prefilled with distilled water, while continually percussing the column sides and top rim with a crescent wrench. We were careful not to tamp the sand directly in order to avoid creating heterogeneous porosity pockets. The average sediment porosity (n) was determined to be 0.37 based on triplicate measurements made via the bulk density method using 100 mL graduated cylinders (Driscoll, 1986). The unpacked and packed column pore volumes (PV) were 623 mL and 228 mL, respectively.

The average measured hydraulic conductivity was 3.0 cm/min (range 2.9-3.11 cm/min). This was calculated by performing three constant head permeameter tests (Model 3891, KarolWarner, Powel OH, USA) averaged using different head differences (Freeze and Cherry, 1979; Weight, 2008). Detailed sediment characteristics, the exact packing procedure, and procedures to measure porosity and hydraulic conductivity are presented in the supplemental information **(**Appendix S1**)**.

Artificial groundwater (AGW) was contained 3.07 mmol/L Cl^-, 5.31 mmol/L HCO_3^-, 0.0774 mmol/L Br^-, and 1.10 mmol/L SO_4^{2-}, and artificial surface water contained 5.33 mmol/L HCO_3^- Both AGW and ASW were prepared using reagent grade or better $NaHCO_3$, KBr, NaCl, and Na_2SO_4 salts, respectively, and distilled water.

Dissolved Cl^-, Br^-, and SO_4^{2-} were assumed to behave conservatively in the sand column. Dissolved Cl^-, Br^-, and SO_4^{2-} concentrations in both influent and effluent samples were measured by ion chromatography with a Metrohm 930 IC Flex using anion column Metrosep A Supp 5

(Metrohm, 2020; Pfaff, 1993). Measured electrical conductance of AGW and ASW were 102.7 µS/cm and 566.3 µS/cm, respectively, at a temperature of 22.5 °C. The room temperature was kept nearly constant (± 0.5 ºC). Therefore, it was not necessary to assume a value for the temperature compensation factor to convert to specific conductance (SC) (McCleskey et al.. 2013). These were measured using the same in-line flow cell that measured effluent EC. This probe was calibrated at the start of each experiment.

Experiment Conditions

The RCF and RVF experiments were run for 24 hr. During this time flow direction was switched every 6 hours, generating two 12 hr periods or four 6 hr half-periods. Within these two periods there were three flow reversal events which occurred at hours 6, 12 and 18 (Fig. 1c-d). The RCF experiment utilized a constant flow rate of 1.23 mL/min whereas the RVF experiment sine wave flow rate ranged from 0.005-2.03 mL/min (Fig. 1c). Over each 6 hr half-period, 2 PV of either AGW or ASW was injected into opposing ends of the column. Thus, a total of 8 PVs were injected over the course of each experiment. During the first and third half-periods, AGW was injected. During the second and fourth half-periods, ASW was injected into the opposite end of the column. Effluent samples were collected in 15 mL falcon tubes with a fraction collector (SuperFrac, Pharmacia, Stockholm, Sweden) at twelve- and eight-minute intervals for the RCF and RVF experiments, respectively. The Arduino codes for the RCF and RVF experiments are provided in the supplemental material **(**Appendix S2**)**.

Simulating Effluent Breakthrough Curves

The observed breakthrough curves of Cl^-, Br^-, and SO_4^{2-} were fit to simulated BTC to estimate dispersivity (α) utilizing the software HYDRUS-1D (Simunek et al., 1998). This allowed the value of dispersivity and sediment Peclet numbers to be compared between the RCF and RVF experiments. Both experiments should produce effectively identical dispersivity estimates with the same sand column, which can test how accurately the apparatus can simulate transient flow regimes with respect to the RCF as a benchmark. Peclet numbers can test whether solutes experience the transition between diffusion and dispersion dominated transport in the low velocity interval as flow begins to ramp up and finishes ramping down at the beginning and end of tidal pulses.

The mathematical representation utilized a 20 cm long 1-D column. Volumetric fluxes from the R1D apparatus were converted to Darcy velocities (Darcy, 1856). The mathematical model boundary conditions consisted of two variable flux boundaries on opposite ends of the column. In the mathematical model, flow was kept the same direction permit model convergence and for simplicity. Flow reversals were simulated by alternating the influent tracer concentration between AGW and ASW composition.. Using unidirectional flow in the model was justified since complete chloride tracer breakthrough was expected and indeed observed after two pore volumes of AGW and ASW were injected into the column over each 6 hr half-period. The RCF mathematical model assumed a constant of 56.8 cm/d throughout the 24 hr experiment. This corresponds to a pore-water residence time of about 2.96 hr. In contrast, the RVF model varied flux from 0-93.9 cm/d as a sinewave that was discretized over 5 min intervals. This corresponds to a pore-water residence time of about 3.01 hr The AGW and ASW injections were simulated by alternating between boundary conservative tracer concentrations of $C/C_o = 1$ and $C/C_o = 0$,

respectively, which alternated at the 6 hr half-periods. Best-fit dispersivity values were estimated with the Marquardt-Levenberg parameter estimation technique built into HYDRUS-1D.

Results & Discussion

Apparatus Performance

One way to assess the degree of accuracy and control of the experimental operating conditions is to compare expected to actual recovered water mass exiting the column. Water mass percent recoveries were 99.2% and 97.9% for the RCF and RVF experiments, respectively. The working volumetric flow range during the RVF experiment was 0.01-2.03 mL/min. The standard errors of the AGW and ASW pump calibration curves were 0.003 mL/min and 0.01 mL/min, respectively, indicating high precision control. Therefore, mass recoveries and calibration curves precision demonstrate accurate fluxes were rigorously maintained throughout the experiment.

The parameters pH, ORP, and temperature maintained stable levels of 7.5-8.0, 329-332 mV, and 22-24°C, respectively **(**Fig. S4**).** The in-line EC probe tracked the sum of dissolved ion transport. This is described in the subsequent section.

Breakthrough Curve Description and Modeling Results

Normalized Cl^- and Br^- BTCs were effectively identical for both the RCF (Fig. 2) and RVF experiments (Fig. 3). Only the Cl^- breakthrough curves are presented in the main paper. The Br^- and SO_4^{2-} breakthrough curves and tabulated data are presented in the supplemental material **(**Fig. S5; Table S2**)**. The breakthrough curve SO_4^{2-} concentrations decreased over the experiment

duration, which may be due to adsorption to Fe-oxides in the column sand (Dzomback and Morel 1990; Zhu et al. 2014).

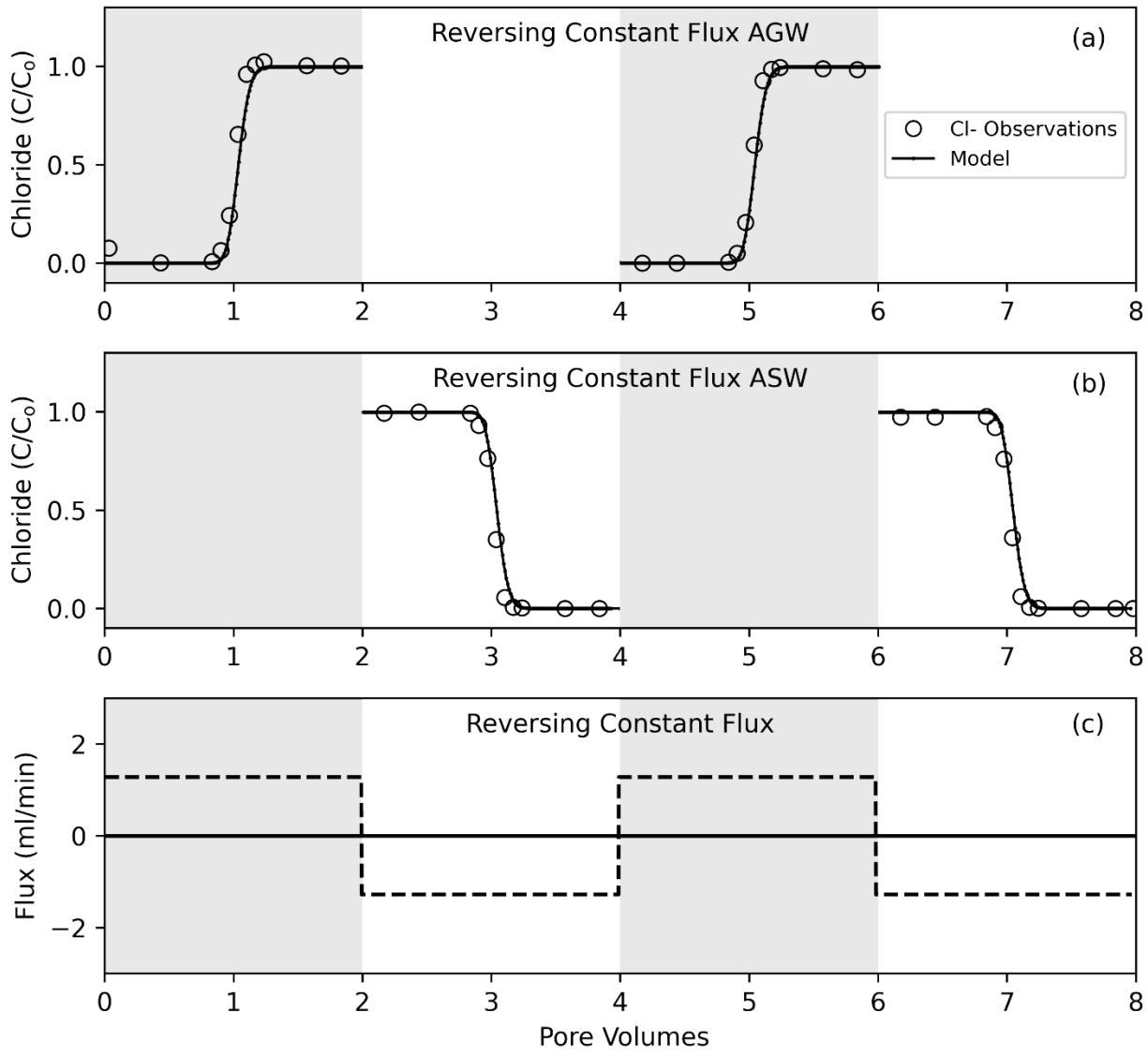

Figure 2. Observed normalized chloride measurements (black circles), best-fit model (solid black line) and flow conditions (hashed line) for the reversing constant flux experiment. (a) Normalized breakthrough curves for Cl^- during AGW injection. Normalized breakthrough curves during ASW injection.(.(c) Flux magnitude and direction. Positive flux indicates AGW injection

into the column. Negative. Negative flux indicates ASW injection into the column. Grey regions indicate flux reversal half-periods when AGW was pumped through the column (0-2 and 4-6 PV). White regions show when ASW was pumped from the opposite end of the column (2-4 and 6-8 PV).

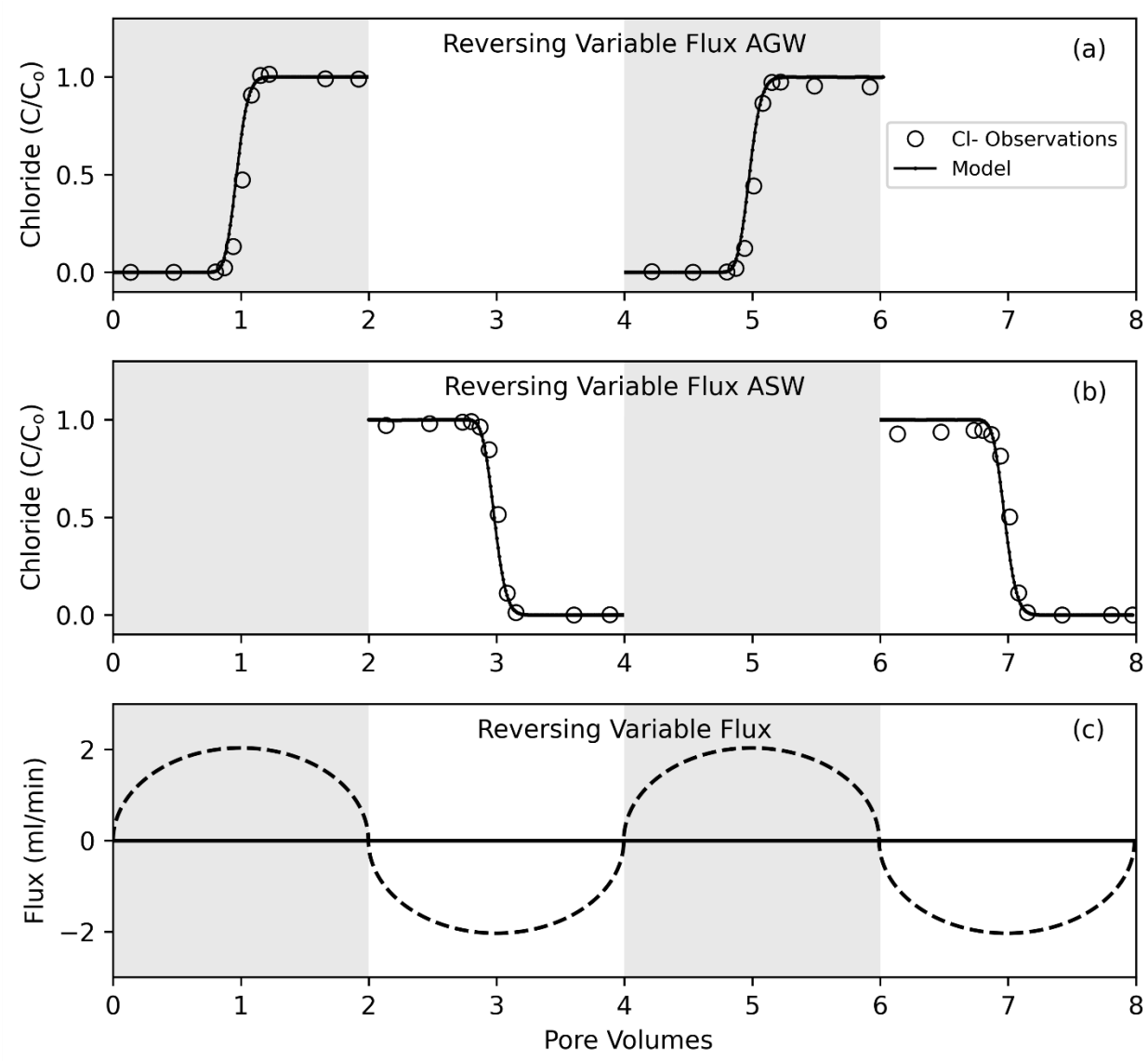

Figure 3. Observed normalized chloride measurements (black circles), best-fits model (solid black line) and flow conditions (hashed line) variable flux experiment. (a) Normalized

breakthrough curves during AGW injection. (b) Normalized breakthrough curves during ASW injection. (c) Flux magnitude and direction. Positive flux indicates AGW injection into the column. Negative flux indicates ASW injection into the column. Grey regions indicate flux reversal half-periods when AGW was pumped through the column (0-2 and 4-6 PV). White). W regions show when ASW was pumped into the opposite end of the column (2-4 and 6-8 PV).

In both the RCF (Fig. 2a2a) and RVF (Fig. 3a3a) experiments the rising limbs of Cl^- breakthrough curves during the first and fifth s during the first and third half-periods correspond to the point where AGW displaces ASW from the column, reaching a plateau at a normalized concentration of 1. During the flow reversal half-periods (2 PV, 4 PV, and 6 PV), complete AGW and ASW breakthrough is observed, and effectively no change in concentration is observed after the reversal until the falling limbs. The falling limbs of Cl^- breakthrough curves at 3 PV and 7 PV correspond to ASW displacing AGW from the column while flowing from the opposite end (Figs. 2b, 3b3b). The assumption that Cl^- is a conservative tracer is justified since the normalized concentration at 1 PV is 0.5, following mean flux, irrespective of the constant and sine wave flux regimes (Figs. 2c, 3c3c) as predicted by the advection-dispersion equation (Bear, 1972).

The best-fit dispersivity values and calculated Peclet numbers are comparable for both RCF and RVF experiments. Dispersivities estimated from the Cl^-, Br^-, and SO_4^{2-} tracers ranged from 0.0454-0.0626 cm and 0.0548-0.101 cm for the RCF and RVF experiments, respectively (Table S2S2). The RVF SO_4^{2-} dispersivity estimate is an outlier, confirmed by the Grubb's test for an outlier (t=7.66) (Grubbs, 1950). These dispersivity estimates are realistic since they are similar to those obtained from other saturated sand column experiments (Tang et al. 2010; Toride

et al. 1995). Dispersivities should be effectively constant, irrespective of flow regime. Comparable dispersivities can only be obtained for the same sediment column if the apparatus can accurately control water flow for the different experiments. Hence the apparatus can accurately simulate different transient flow regimes, including those analogous to real-world tidally fluctuating riverbanks.

Sediment Peclet numbers (Eq.) calculated from the Cl^- dispersivity were 381 for the RCF experiment. In the RVF experiment the Peclet numbers ranged 92.7 to 338 for minimum and maximum fluxes, respectively.

$$P = \frac{l*v}{D_L} = \frac{l*\frac{q}{n}}{\frac{q}{n}*\alpha+\omega D_d} \quad (1)$$

where l is the length of the column, v is average linear velocity, D_L is longitudinal hydrodynamic dispersion, q is linear Darcy velocity, n is porosity, α is dispersivity, ω is tortuosity (0.7), and D_d is coefficient of molecular diffusion, which is assumed to be the average diffusion for Na^+, K^+, Cl^-, Br^-, and SO_4^{2-}, at 25°C for marine sediment porewaters ($1.45*10^{-4}$ m^2/d) (Fetter, 1999; Huysmans and Dassargues, 2005; Perkins and Johnston, 1963; Yuan-Hui and Gregory, 1974). Tortuosity was assumed to be 0.7 based on prior column experiments with uniformly packed sand (Perkins and Johnston, 1963). Peclet numbers for the Br^- and SO_4^{2-} BTC were generally similar and are presented in the supplementary information (Table S3). Sediment Peclet numbers >100 indicate mechanical dispersion (as opposed to molecular diffusion) dominated flow for both experiments at their maximum flow (Freeze and Cherry, 1979; Huysmans and Dassargues, 2005). These large Peclet numbers support the interpretation of conservative tracer behavior with C/Co = 0.5 at 1 PV. In the RVF experiment during the 8 min pause at the during the transition from one direction of flow to the other P =0, indicating purely diffusion dominated transport. In

contrast, at the start and end of each RVF half-period while flow rates are low (q <=0.03 mL/min), competing diffusion and dispersion briefly control contaminant transport. The transition between diffusion and dispersion dominated transport is analogous to transition periods between different tidal pulses. Hence, the apparatus can simulate sensitive physical solute transport behaviors in a sine wave tidal pulse that are comparable to a real-world tidally fluctuating river.

Potential Applications and Limitations

The reversing and changing pore velocities have the potential to mobilize and transport fine particles and colloids (Bedrikovetsky et al., 2012; Bergendahl and Grasso, 2000; Bradford et al.. 2011; Ryan and Gschwend, 1994; Sharma et al.. 1992; Shen et al.. 2012). Once mobilized, these fine particles may collect in pore throats thereby reducing the hydraulic conductivity of the sand over time. During development of the apparatus, ultrafine sand size glass sandblasting beads were tested as a column matrix, but pore throat clogging resulted in complete flow blockage within 5 min of the start of the experiment. The same behavior is expected for soils with significant silt and clay sized particles and/or particularly heterogenous (poorly sorted) sediments of larger grain sizes (Ryan and Gschwend, 1994). For heterogenous sediments, sieving to achieve a sample with a homogenous grain size may be a solution. We also suspect monolith type columns (undisturbed sediment cores) will be susceptible to pore throat clogging. Hence, packed columns may be necessary and add the benefit of improving experiment reproducibility (Lewis and Sjöstrom, 2010). Hence, preparing sediment cores for R1D experiments should be approached with the potential for pore throat clogging in mind on a case-by-case basis, which is beyond the scope of this study.

The apparatus could be subsequently modified to study mixing zones with fluctuating redox gradients. Riverbank mixing zones often exhibit redox gradients controlled by mixing of anerobic groundwaters and aerobic surface waters (Berube et al.... 2018; Bone et al.... 2006; Datta et al. 2009; Hester et al. 2017; Parsons et al. 2013; Sawyer et al. 2009; Xu et al. 2017; Zachara et al. 2013). The redox gradient passing through the column can be monitored with an ORP or DO probe. By mixing anerobic groundwater and aerobic surface water reservoirs, a redox mixing gradient can be simulated.

Conclusions

A novel, programmable reversing flow 1D column with two reservoirs (R1D) experimental apparatus was designed, constructed and tested to simulate dynamic reversing flow regimes. We conducted transient variable flux R1D experiments using conservative tracers in the form of a constant flow with abrupt flow reversals and sine wave with gradual ramping to stagnant conditions before flow reversals. The later mimicking semi-diurnal flow reversals in a riverbank aquifer adjacent to a tidally fluctuating river, demonstrating the ability to simulate real-world systems. Comparable RVF and the control RCF experiment dispersivity estimates demonstrate that the apparatus is capable of simulating complex flow regimes analogous to those in real world environments. Simulating these more complex and realistic flow regimes is important because during the RVF experiment Peclet numbers indicated that solute transport transitioned between diffusion and dispersion dominated transport. A simpler, less accurate flow regime would fail to include periods of diffusion-dominated transport of solutes which may impact reaction kinetics.

This demonstrates the apparatus's potential to simulate highly dynamic reversing flow systems. The apparatus cost $3515.62 USD (2021) to construct. This combined with low cost, opensource software provides an opportunity for more robust simulation of settings with dynamically reversing flow in aquifers. The R1D apparatus should be capable of answering questions on how contaminant transport in sediments along the banks of dynamically fluctuating rivers is jointly influenced by physical flow and biogeochemical reactions generated by reactants within sediments and end-member chemistries. The R1D apparatus can potentially complement field and modeling approaches, providing a bench-scale physical analog to identify important reactions and constrain their kinetics which will help understand contaminant immobilization and mobilization in settings where flow reversals and mixing of disparate chemical compositions.

Acknowledgments & Authorship Attribution

Primary funding for this project was made possible by the National Science Foundation (EAR-1852652) to P. Knappett and the Gould Research Grant through the Geological Society of America Graduate Student Research Grants Program to R. Buskirk. Additional funding to M. B. Cardenas and S. Datta from the National Science Foundation Hydrologic Sciences grant numbers EAR- 1852653 and EAR- 1940772, respectively, is acknowledged. The general study was designed by P. Knappett. The specific apparatus was designed, built, tested, and operated by R. Buskirk with frequent discussions with P. Knappett, M. B. Cardenas and S. Datta. All authors contributed to the writing. W. Borowski at Eastern Kentucky University assisted R. Buskirk with ion chromatography analyses through his laboratory. The authors are grateful for Robert Buskirk who constructed the wood housing box for the apparatus. The authors furthermore thank J.

Buskirk, S. Lynch, and C. Midkiff for their advice to R. Buskirk on electronics during the construction of the apparatus. Aaron Pena Rodriguez is thanked for creating the Solidworks files for the flow cells which were built for the apparatus by W. Seward in the Texas A&M Department of Chemistry Machine Shop. The authors are grateful for advice on Peclet numbers and dispersivity from Dr. Hongbin Zhan. The authors are grateful for the proofreading assistance of Selsey Stribling.

Authors' Note: The author(s) declare that they have no conflicts of interest.

Supporting Information

Additional Supporting Information may be found in an online document that contains figures S1-S5, Tables S1-3, and Appendixes S1-2 as referenced in the text above. The supporting information is generally *not* peer reviewed.

References

Bear, J. 1972. Dynamics of fluids in porous media. New York: Dover.

Bearup, L. A., A. K. Navarre-Sitchler, R. M. Maxwell, and J. E. McCray. 2012. Kinetic metal release from competing processes in aquifers. *Environmental Science and Technology* 46, no. 12: 6539–47 DOI: 10.1021/es203586y

Bedrikovetsky, P., A. Zeinijahromi, F. D. Siqueira, C. A. Furtado, and A. L. S. de Souza. 2012. Particle detachment under velocity alternation during suspension transport in porous media. *Transport in Porous Media* 91, no. 1: 173–97.

Benner, S. G., M. L. Polizzotto, B. D. Kocar, S. Ganguly, K. Phan, K. Ouch, M. Sampson, and S. Fendorf. 2008. Groundwater flow in an arsenic-contaminated aquifer, Mekong Delta, Cambodia. *Applied Geochemistry* 23, no. 11: 3072–87.

Bergendahl, J., and D. Grasso. 2000. Prediction of colloid detachment in a model porous media: hydrodynamics. *Chemical Engineering Science* 55, no. 9: 1523–32.

Berner, R. A. 1978. Rate control of mineral dissolution under earth surface conditions. *American Journal of Science* 278, no. 9: 1235–52.

Berube, M., K. Jewell, K. D. Myers, P. S. K. Knappett, P. Shuai, A. Hossain, M. Lipsi, et al. 2018. The fate of arsenic in groundwater discharged to the Meghna River, Bangladesh. *Environmental Chemistry* 15, nos. 1–2: 29–45 DOI: 10.1071/EN17104

Bone, S. E., M. E. Gonneea, and M. A. Charette. 2006. Geochemical cycling of arsenic in a coastal aquifer. *Environmental Science and Technology* 40, no. 10: 3273–78 DOI: 10.1021/es052352h

Bradford, S. A., S. Torkzaban, and A. Wiegmann. 2011. Pore-scale simulations to determine the applied hydrodynamic torque and colloid immobilization. *Vadose Zone Journal* 10, no. 1:

252–61.

Brush, C. F., W. C. Ghiorse, L. J. Anguish, J.-Y. Parlange, and H. G. Grimes. 1999. Transport of Cryptosporidium parvum oocysts through saturated columns.

Darcy, H. 1856. *Les fontaines publiques de la ville de Dijon: exposition et application.* Paris: Libraire des Corps imperiaux des ponts et chaussees et des mines.

Datta, S., B. Mailloux, H. B. Jung, M. A. Hoque, M. Stute, K. M. Ahmed, and Y. Zheng. 2009. Redox trapping of arsenic during groundwater discharge in sediments from the Meghna riverbank in Bangladesh. *Proceedings of the National Academy of Sciences of the United States of America* 106, no. 40: 16930–35 DOI: 10.1073/pnas.0908168106.

Drever, J. I. 1997. *The geochemistry of natural waters Prentice Hall*. *Englewood Cliffs, New Jersey*. 3rd ed.

Driscoll, F. G. 1986. *Groundwater and wells 2nd edn*. Johnson Division, St. Paul.

Dzombak, D. A., and F. M. M. Morel. 1990. *Surface complexation modeling: hydrous ferric oxide*. John Wiley & Sons.

Fetter, C. W. 1999. *Contaminant hydrogeology 2nd-edn*. Hilton Head Island: Waveland Press, Inc.

Freeze, R. A., and J. A. Cherry. 1979. *Groundwater.* Englewood Cliffs: Prentice-Hall.

Geng, X., J. W. Heiss, H. A. Michael, H. Li, B. Raubenheimer, and M. C. Boufadel. 2021. Geochemical fluxes in sandy beach aquifers: Modulation due to major physical stressors, geologic heterogeneity, and nearshore morphology. *Earth-Science Reviews* 221: 103800.

Grubbs, F. E. 1950. Sample criteria for testing outlying observations. *The Annals of Mathematical Statistics*, 27–58.

Huang, Y., P. S. K. Knappett, M. Berube, S. Datta, M. B. Cardenas, K. A. Rhodes, N. T. Dimova, I. Choudhury, K. M. Ahmed, and A. van Geen. 2022. Mass fluxes of dissolved arsenic discharging to the Meghna River are sufficient to account for the mass of arsenic in riverbank sediments. Journal of Contaminant Hydrology 251: 104068.

Hester, E. T., M. B. Cardenas, R. Haggerty, and S. V Apte. 2017. The importance and challenge of hyporheic mixing. *Water Resources Research* 53, no. 5: 3565–75.

Huysmans, M., and A. Dassargues. 2005. Review of the use of Péclet numbers to determine the relative importance of advection and diffusion in low permeability environments. *Hydrogeology Journal* 13, no. 5: 895–904.

Jung, H. B., Y. Zheng, M. W. Rahman, M. M. Rahman, and K. M. Ahmed. 2015. Redox zonation and oscillation in the hyporheic zone of the Ganges-Brahmaputra-Meghna Delta: Implications for the fate of groundwater arsenic during discharge. *Applied Geochemistry* 63: 647–60, https://doi.org/10.1016/j.apgeochem.2015.09.001.

Kim, K. H., J. W. Heiss, H. A. Michael, W.-J. Cai, T. Laattoe, V. E. A. Post, and W. J. Ullman. 2017. Spatial patterns of groundwater biogeochemical reactivity in an intertidal beach aquifer. *Journal of Geophysical Research: Biogeosciences* 122, no. 10: 2548–62.

Knappett, P. S. K., M. B. Emelko, J. Zhuang, and L. D. McKay. 2008. Transport and retention of a bacteriophage and microspheres in saturated, angular porous media: Effects of ionic strength and grain size. *Water Research* 42, no. 16: 4368–78.

Kruisdijk, E., and B. M. van Breukelen. 2021. Reactive transport modelling of push-pull tests: A versatile approach to quantify aquifer reactivity. *Applied Geochemistry* 131: 104998.

Laing, G. Du, E. Meers, M. Dewispelaere, J. Rinklebe, B. Vandecasteele, M. G. Verloo, and F. M. G. Tack. 2009. Effect of water table level on metal mobility at different depths in

wetland soils of the Scheldt Estuary (Belgium). *Water, air, and soil pollution* 202, no. 1: 353–67.

Lewis, J., and J. Sjöstrom. 2010. Optimizing the experimental design of soil columns in saturated and unsaturated transport experiments. *Journal of Contaminant Hydrology* 115, nos. 1–4: 1–13 DOI: 10.1016/j.jconhyd.2010.04.001

Li, Y., J. Zhu, L. Wang, Y. Gao, W. Zhang, H. Zhang, and L. Niu. 2020. Grain size tunes microbial community assembly and nitrogen transformation activity under frequent hyporheic exchange: A column experiment. *Water Research*, 116040.

Liu, Y., C. Liu, W. C. Nelson, L. Shi, F. Xu, Y. Liu, A. Yan, et al. 2017. Effect of water chemistry and hydrodynamics on nitrogen transformation activity and microbial community functional potential in hyporheic zone sediment columns. *Environmental science \& technology* 51, no. 9: 4877–86.

McAllister, S. M., J. M. Barnett, J. W. Heiss, A. J. Findlay, D. J. MacDonald, C. L. Dow, G. W. Luther III, H. A. Michael, and C. S. Chan. 2015. Dynamic hydrologic and biogeochemical processes drive microbially enhanced iron and sulfur cycling within the intertidal mixing zone of a beach aquifer. *Limnology and Oceanography* 60, no. 1: 329–45.

McCleskey, R. B. 2013. New method for electrical conductivity temperature compensation. *Environmental Science and Technology* 47, no. 17: 9874–81, https://doi.org/10.1021/es402188r.Metrohm. 2020. *Manual 8.107.8050. Column Manual Metrosep A Supp 5 (6.1006.XX0)*, Herisau: Metrohm https://www.metrohm.com/content/metrohm/en/products/8/1078/81078040.html.

Michael, H. A., J. S. Lubetsky, and C. F. Harvey. 2003. Characterizing submarine groundwater discharge: A seepage meter study in Waquoit Bay, Massachusetts. *Geophysical Research*

Letters 30, no. 6.

Nkedi-Kizza, P., J. W. Biggar, H. M. Selim, M. T. Van Genuchten, P. J. Wierenga, J. M. Davidson, and D. R. Nielsen. 1984. On the equivalence of two conceptual models for describing ion exchange during transport through an aggregated oxisol. *Water Resources Research* 20, no. 8: 1123–30.

Parsons, C. T., R. M. Couture, E. O. Omoregie, F. Bardelli, J. M. Greneche, G. Roman-Ross, and L. Charlet. 2013. The impact of oscillating redox conditions: Arsenic immobilisation in contaminated calcareous floodplain soils. *Environmental Pollution* 178: 254–63, https://doi.org/10.1016/j.envpol.2013.02.028.

Perkins, T. K., and O.C. Johnston. 1963. A review of diffusion and dispersion in porous media. *Society of Petroleum Engineers Journal* 3, no. 01: 70–84.

Pfaff, J. D. 1993. EPA Method 300.0: Determination of inorganic anions by ion chromatography. Cincinati: U.S. Environmental Protection Agency

Radloff, K. A., Y. Zheng, H. A. Michael, M. Stute, B. C. Bostick, I. Mihajlov, M. Bounds, et al. 2011. Arsenic migration to deep groundwater in Bangladesh influenced by adsorption and water demand. *Nature Geoscience* 4, no. 11: 793–98.

Radloff, K. A., Y. Zheng, M. Stute, B. Weinman, B. Bostick, I. Mihajlov, M. Bounds, et al. 2017. Reversible adsorption and flushing of arsenic in a shallow, Holocene aquifer of Bangladesh. *Applied Geochemistry* 77: 142–57.

Rezanezhad, F., R.-M. Couture, R. Kovac, D. O'Connell, and P. Van Cappellen. 2014. Water table fluctuations and soil biogeochemistry: An experimental approach using an automated soil column system. *Journal of Hydrology* 509: 245–56.

Rhodes, K. A., T. Proffitt, T. Rowley, P. S. K. Knappett, D. Montiel, N. Dimova, D. Tebo, and

G. R. Miller. 2017. The importance of bank storage in supplying baseflow to rivers flowing through compartmentalized, alluvial aquifers. *Water Resources Research* 53, no. 12: 10539–57.

Ryan, J. N., and P. M. Gschwend. 1994. Effects of ionic strength and flow rate on colloid release: Relating kinetics to intersurface potential energy. *Journal of colloid and interface science* 164, no. 1: 21–34.

Sather, L. J., Roth, E. J., Neupauer, R. M., Crimaldi, J. P., and Mays, D. C., 2023. Experiments and simulations on plume spreading by engineered injection and extraction in refractive index matched porous media. *Water Resources Research* 59 DOI: 10.1029/2022WR032943

Sawyer, A. H., M. B. Cardenas, A. Bomar, and M. Mackey. 2009. Impact of dam operations on hyporheic exchange in the riparian zone of a regulated river. *Hydrological Processes: An International Journal* 23, no. 15: 2129–37.

Sharma, M. M., H. Chamoun, D. S. H. S. R. Sarma, and R. S. Schechter. 1992. Factors controlling the hydrodynamic detachment of particles from surfaces. *Journal of colloid and interface science* 149, no. 1: 121–34.

Shen, C., V. Lazouskaya, H. Zhang, F. Wang, B. Li, Y. Jin, and Y. Huang. 2012. Theoretical and experimental investigation of detachment of colloids from rough collector surfaces. *Colloids and Surfaces A: Physicochemical and Engineering Aspects* 410: 98–110.

Shuai, P., P. S. K. Knappett, S. Hossain, A. Hosain, K. Rhodes, K.Ahmed, and M. B. Cardenas. 2017. The impact of the degree of aquifer confinement and anisotropy on tidal pulse propagation. *Groundwater* 55, no. 4: 519–31.

Simunek, J., M. Sejna, M. T. Van Genuchten, J. Šimuunek, M. Šejna, D. Jacques, J. Šimunek, D. Mallants, H. Saito, and M. Sakai. 1998. HYDRUS-1D. *Simulating the one-dimensional*

movement of water, heat, and multiple solutes in variably-saturated media, version 2. PC Progress, Prague, Czech Republic.

Spiteri, C., C. P. Slomp, M. A. Charette, K. Tuncay, and C. Meile. 2008. Flow and nutrient dynamics in a subterranean estuary (Waquoit Bay, MA, USA): field data and reactive transport modeling. *Geochimica et Cosmochimica Acta* 72, no. 14: 3398–3412.

Tang, G., Mayes, M. A., Parker, J. C., and Jardine, P. M. 2010. CXTFIT/Excel—a modular adaptable code parameter estimation, sensitivity analysis and uncertainty analysis for laboratory or field tracer experiments. *Computers & Geosciences*, 36(9), 1200-1209

Tatham, S. 2021. puTTY 0.76, https://www.chiark.greenend.org.uk/~sgtatham/putty/.

Teutsch, N., U. von Gunten, D. Porcelli, O. A. Cirpka, and A. N. Halliday. 2005. Adsorption as a cause for iron isotope fractionation in reduced groundwater. *Geochimica et Cosmochimica Acta* 69, no. 17: 4175–85 DOI:10.1016/j.gca.2005.04.007.

Toride, N., Leij, F. J., and van Genuchten M. Th. 1995. *The CXTFIT code for estimating transport parameters from laboratory or filled tracer experiments*, Vol 2. Riverside, CA: US Salinity Laboratory.

Wang, Y., H. Wang, J.-S. He, and X. Feng. 2017. Iron-mediated soil carbon response to water-table decline in an alpine wetland. *Nature communications* 8, no. 1: 1–9.

Weight, W. D. 2008. *Hydrogeology Field Manual*. 2nd ed. New York: McGraw Hill.

Xin, P., S. S. J. Wang, C. Shen, Z. Zhang, C. Lu, and L. Li. 2018. Predictability and quantification of complex groundwater table dynamics driven by irregular surface water fluctuations. *Water Resources Research* 54, no. 3: 2436–51.

Xu, F., Y. Liu, J. Zachara, M. Bowden, D. Kennedy, A. E. Plymale, and C. Liu. 2017. Redox transformation and reductive immobilization of Cr (VI) in the Columbia River hyporheic

zone sediments. *Journal of Hydrology* 555: 278–87.

Yuan-Hui, L., and S. Gregory. 1974. Diffusion of ions in sea water and in deep-sea sediments. *Geochimica et cosmochimica acta* 38, no. 5: 703–14.

Zachara, J. M., P. E. Long, J. Bargar, J. A. Davis, P. Fox, J. K. Fredrickson, M. D. Freshley, et al. 2013. Persistence of uranium groundwater plumes: contrasting mechanisms at two DOE sites in the groundwater--river interaction zone. *Journal of contaminant hydrology* 147: 45–72.

Zhu, M., P. Northrup, C. Shi, S. J. L. Billinge, D. L. Sparks, and G. A. Waychunas. 2014. Structure of sulfate adsorption complexes on ferrihydrite. *Environmental Science & Technology Letters* 1, no. 1: 97–101.

Ziliotto, F., M. B. Hazas, M. Rolle, and G. Chiogna. 2021. Mixing enhancement mechanisms in aquifers affected by hydropeaking: Insights from flow-through laboratory experiments. *Geophysical Research Letters*, e2021GL095336.

Figure Captions List

Figure 1. Tubing connections and flow pathways within the R1D apparatus are illustrated. Artificial groundwater and artificial surface water chemistries are represented by the colors red and blue, respectively. (a) Artificial groundwater injection stage. (b) Artificial injection stage following a reversal in flow direction. (c) Two different flow regimes approximating tidal pulse signal. The constant and variable flux regime temporal pattern in flux (and driving head) are represented by purple and blue, respectively. (d) Conceptual model that shows the location of the sediment column in the riverbank and the hydraulic gradients during gaining and losing conditions.

Figure 2. Observed normalized chloride measurements (black circles), best-fit model (solid black line) and flow conditions (hashed line) for the reversing constant flux experiment. (a) Normalized breakthrough curves for Cl^- during AGW injection. Normalized breakthrough curves during ASW injection.(.(c) Flux magnitude and direction. Positive flux indicates AGW injection into the column. Negative. Negative flux indicates ASW injection into the column. Grey regions indicate flux reversal half-periods when AGW was pumped through the column (0-2 and 4-6 PV). White regions show when ASW was pumped from the opposite end of the column (2-4 and 6-8 PV).

Figure 3. Observed normalized chloride measurements (black circles), best-fits model (solid black line) and flow conditions (hashed line) variable flux experiment. (a) Normalized breakthrough curves during AGW injection. (b) Normalized breakthrough curves during ASW injection. (c) Flux magnitude and direction. Positive flux indicates AGW injection into the column. Negative flux indicates ASW injection into the column. Grey regions indicate flux reversal half-periods when AGW was pumped through the column (0-2 and 4-6 PV). White). W regions show when ASW was pumped into the opposite end of the column (2-4 and 6-8 PV).